Large photostriction near the phase boundary in $BiFeO_3$ under varying epitaxial strain

Yali Yang,[1,*] Carmel Dansou,[2] Charles Paillard,[2,3] Jiangang He,[1] Hongjun Xiang,[4] and Laurent Bellaiche[2,†]
[1]*School of Mathematics and Physics, University of Science and Technology Beijing, Beijing 100083, China*
[2]*Smart Ferroic Materials Center, Institute for Nanoscience & Engineering and Department of Physics,*
University of Arkansas, Fayetteville, Arkansas 72701, USA
[3]*Université Paris-Saclay, CentraleSupélec, CNRS, Laboratoire SPMS, 91190 Gif-sur-Yvette, France*
[4]*Key Laboratory of Computational Physical Sciences (Ministry of Education), Institute of Computational Physical Sciences,*
and Department of Physics, Fudan University, Shanghai 200433, China

(Received 11 March 2024; accepted 13 May 2024; published 29 May 2024)

Controlling the structure and properties of perovskite materials through various handles has always been an important research direction. In this present study, constrained density functional theory calculations are performed to systematically investigate the impact of illumination on the so-called *R* and the *T* phases of strained $BiFeO_3$ film under different epitaxial biaxial strains. We find that the phase transition strain boundary between the two phases is barely affected by illumination. However, it is discovered that light can induce a noticeable change in the two phases population, and that both the *R* and the *T* phases are strongly photostrictive near the phase transition boundary, with such photostriction being mainly accounted for by a converse piezoelectric model. The results of our calculations reveal the exciting prospect of using strained phases of $BiFeO_3$ for photostrictive applications. This combined with their known functional behavior could lead to devices with exotic cross functionality.

DOI: 10.1103/PhysRevB.109.184111

I. INTRODUCTION

The control of structural and other physical properties of perovskite materials is of fundamental and technological interest. It has been achieved by various approaches, such as uniaxial and biaxial strains, hydrostatic pressure, chemical doping, and magnetic and electric fields [1–8]. For instance, structural phase transitions can happen under strain, during which the performance of the perovskite systems can be adjusted, and new properties can even appear. Examples include induction of electric polarization or magnetization [8,9]. More recently, several works have pointed out that light may be a new effective way to tune properties of materials, for example, resulting in structural [10], insulator-metal [11], magnetic [12], and topological phase transitions [13,14], as well as photoinduced strain [15,16] and generating so-called hidden phases [17,18] and even switching ferroelectricity [19–21].

As one of the most important and widely studied multiferroic materials, $BiFeO_3$ (BFO) exhibits great application potential in emerging electronic devices due to its outstanding coupled optical, electrical, and magnetic properties. Previous experimental and computational works have indicated that $BiFeO_3$ could exhibit several structural phases, in general, and the so-called *R* and *T* phases, in particular, when varying physical handles such as the amount of strain arising from the substrate on top of which BFO films are grown. The *R* phase shows smaller polarization and antiphase octahedral tilting along the [111] direction of the pseudocubic cell. In contrast, the *T* phase presents a large polarization that nearly lies along the [001] direction as well as a much larger *c*/*a* axial ratio than the *R* phase [22–25]. Strikingly, these two phases have different optical, electronic, elasto-optic, piezoelectric, and dielectric properties [24–28].

Up to now, the transition between the *T* and *R* phases has been mainly accomplished by applying biaxial strain, electric field, and uniaxial stress. During these processes, the ratio of the *T* and *R* phases within the same sample can be tuned [2,29–31]. It is also worth noting that one of the current research interests resides in the light-induced lattice deformation (or light-induced nonthermal strain), which is defined as the photostriction effect. It has been reported in several materials, and is promising for future electronic devices [15,16,32–35]. In bulk $BiFeO_3$, photostriction has been reported to induce a large shear strain [35,36], and its microscopic mechanism is the screening of the spontaneous polarization by the photoexcited electrons in combination with the inverse piezoelectric effect [35]. In view of the excellent control ability of strain and light field on materials, it is timely to wonder if the structural and other properties of $BiFeO_3$ films can be controlled and greatly optimized under the combined effect of a light field and in-plane biaxial strain.

Here, such combined effect on the energetics and properties of the *R* and *T* phases of $BiFeO_3$ is studied using an original *ab initio* approach with constrained electronic occupation numbers [10,33,35]. We find that the *T* and *R* phases can coexist under a certain range of in-plane lattice constants and light intensity, the ratio of the two phases being tunable under this dual control of strain and light. We also discover

---

[*] ylyang@ustb.edu.cn
[†] laurent@uark.edu

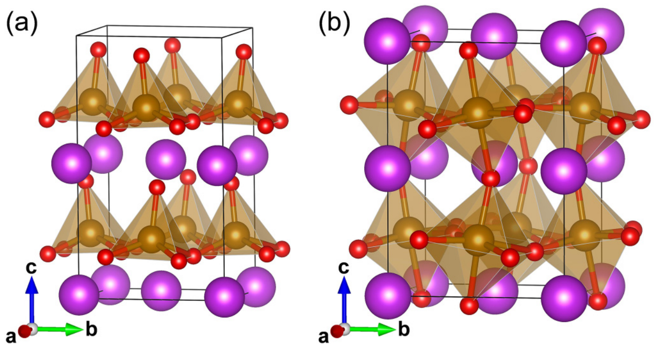

FIG. 1. Schematization of the crystal structure of the *T* (left side) and *R* (right side) phases of $BiFeO_3$ adopted in our calculations.

a large photostriction for the *R* and *T* phases near the phase transition boundary between such *R* and *T* phases. A model is further proposed and successfully tested, which allows us to explain the mechanism behind such large photostriction, as well as other effects of the combined effect of strains and lights on various properties of the *R* and *T* phases of BFO films.

The paper is organized as follows. Section II describes the methods we adopted when performing simulations, and the detailed explanation about how the strain and illumination are applied in the simulations. The calculated results and detailed discussions about the results are provided in Sec. III. Finally, Sec. IV concludes this paper.

II. METHODS

Density functional theory (DFT) calculations are performed using the ABINIT software package [37–40] within the projector augmented-wave framework [41]. The local spin density approximation + U [42] functional is used with $U =$ 3.87 eV [35]. The wave functions are expanded using plane-wave basis sets with a kinetic energy cutoff of 35 hartree. As shown in Fig. 1, a 20-atom, $\sqrt{2} \times \sqrt{2} \times 2$ supercell is employed for both the *R* and the *T* phases. An unshifted $8 \times 8 \times 6$ k-point grid is used here for these two phases. Structural convergence is achieved until the force on any atoms is less than 1×10^{-6} hartree/bohr. In our simulations, the (pseudocubic) in-plane lattice constants of these phases are allowed to vary from $a = b = 3.60$ to 3.92 Å, which covers a large but realistic range and can involve various substrates providing different biaxial misfit strains [e.g., $SmScO_3$ (misfit strain of +0.5%), $SrTiO_3$ (misfit strain of −1.6%), $LaAlO_3$ (misfit strain of −4.5%), and $YAlO_3$ (misfit strain of −7%)] [43–45]. At each selected in-plane lattice constant and for the case of both dark and illumination conditions, the (pseudocubic) out-of-plane constant c, as well as the α and β angles (which are the angle between the b and c axes and the angle between the c and a axes, respectively) and the atomic positions are free to relax. In contrast, the in-plane lattice constant and the γ angle (which is the angle between the a and b axes) are fixed during the relaxation. The application of the light to the *R* and *T* phases is modeled by a recently developed constrained density functional theory method [10,33,35,38,46], which provides a certain concentration of electrons into excited states, leaving holes in the valence bands. Practically, such concentration, to be denoted as n_{ph}, is chosen to vary from 0 to 0.2 electron/formula unit (e/f.u.). Such latter concentration is estimated to correspond to 3×10^{21} e/cm^3, which is higher than the current experimentally largest value of $5 \times 10^{19-20} e/\mathrm{cm}^3$ in BFO [36] but is smaller in magnitude than the typical values $10^{22}-10^{23}$ e/cm^3 in metals as well as those adopted in some theoretical works for inorganic systems, such as GaAs [47], bilayer MoS_2 [48], and $BaTiO_3$ (and $PbTiO_3$) [10]. Fermi-Dirac distributions with a smearing temperature of 0.003 Ha are presently adopted. The electric polarization is calculated via the Born effective charge method. Since we investigate low concentrations of photoexcited carriers (0–0.2 e/f.u.), we do not anticipate that the Born effective charges would be heavily modified. Indeed, the conduction and valence bands being mostly Fe $3d$ and O $2p$ states, respectively [49], and assuming that all photoexcited carriers are transferred from O $2p$ to Fe $3d$, one can anticipate that the Born effective charges of Fe is reduced at most by 5.76% and O by 2.56%, which is much smaller than the observed change of polarization in Fig. 5. One could also employ the generalized framework developed in Ref. [50] to obtain more accurate Born effective charges under illumination. The density functional perturbation theory (DFPT) method [37,40] is performed to compute the piezoelectric and elastic tensors in dark conditions. All the calculations are performed at 0 K, thus no temperature effect is presently considered.

III. RESULTS AND DISCUSSION

The energy curves as a function of the in-plane lattice constant under varying concentrations of photoexcited carrier pairs are shown in Fig. 2(a), for both the *T* and the *R* phases. Without light, the *T* phase adopts a minimum at a relatively small in-plane lattice constant $a = 3.72$ Å, while the *R* phase also exhibits a minimum in energy but for a larger in-plane lattice constant $a = 3.90$ Å. Furthermore, interpolating the energy curves of the *T* and *R* phases leads to a crossing between $a = 3.72$ and 3.74 Å, which corresponds to compressive strains between 4.10% and 4.65% with respect to the in-plane lattice constant of the ground state. All these features are consistent with previous experimental and theoretical works [22–24,51]. Interestingly, when applying light on both the *T* and the *R* phases, these two energy curves barely change in shape, but rather simply move up when more electrons are excited. Consequently, the light intensity has basically no significant effect on the crossing point between the *T* and *R* phases; that is, such (interpolated) point occurs between $a = 3.72$ Å and $a = 3.74$ Å for any chosen n_{ph}.

Previous works have shown that, in fact, a mixture of the *T* and *R* phases can simultaneously appear in $BiFeO_3$ films under some epitaxial conditions and for some specific thicknesses [2,25,28,52–54]. Furthermore, the population of the *R* and *T* phases in this mixed phase structure can be tuned via, e.g., the application of stress or electric fields [2,26,53,55]. In order to investigate whether the population of the *R* and *T* phases can also be controlled via light and biaxial strains in the mixed structure, we decided to adopt the common tangent method, which is regularly employed in the analysis of mixed phase regions in conventional phase diagrams [2,56].

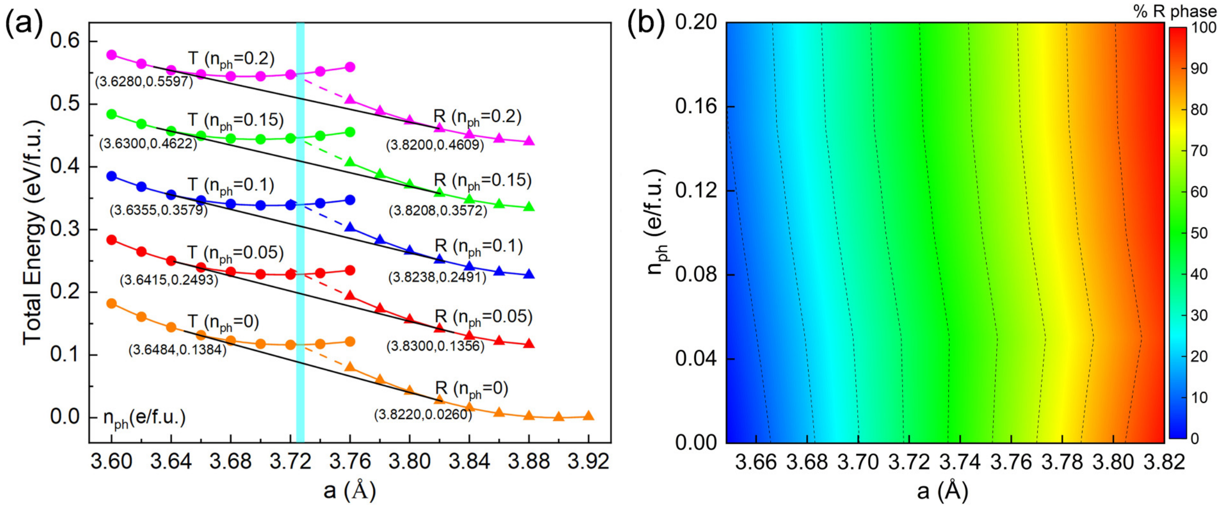

FIG. 2. Schematic of energetics and occupation ratio of the R and T phases of $BiFeO_3$ under biaxial strain and light. (a) Energy curves as a function of the in-plane lattice constant under varying concentrations of photoexcited carrier pairs n_{ph} (e/f.u.). (b) Graphical representation showing the continuous variation in the proportion of the R phase (x_R) with the in-plane lattice constant and photoexcited carrier pairs. Note that $0 \leqslant x_R \leqslant 1$, with the limiting values of $x_R = 0$ and $x_R = 1$ occurring when $a_i < a_T$ and $a_i > a_R$, respectively (see text). The vertical strip in cyan color indicates the phase boundary between the R and T phases of $BiFeO_3$ under varying intensities of light.

Technically and similarly to Ref. [2], the so-called "lever rule" is applied individually for each value of n_{ph}: first, the common tangent for each pair of energy curves is drawn [as shown in Fig. 2(a)], which allows one to extract the a_R and a_T in-plane lattice parameters where the tangent intersects the R and T energy curves, respectively. Then the relative proportion of the R phase, x_R, and consequently of the T phase, x_T, for any a_i in-plane lattice constant being located between a_R and a_T is calculated via

$$x_R = 1 - x_T = \frac{a_i - a_T}{a_R - a_T}. \tag{1}$$

The resulting computed phase population diagram is shown in Fig. 2(b). For any n_{ph}, the R phase is predominant for larger in-plane lattice constants, while mostly the T phase is expected to occur at smaller in-plane lattice constants. It is also worthwhile to realize that the light can also slightly change the phase population, especially when the in-plane lattice constant is around $a = 3.685$ and 3.775 Å, which are values 0.035 and 0.055 Å smaller and larger, respectively, from the interpolated crossing transition point of around $a = 3.72$ Å. For example, the x_R value at $a_i = 3.685\,(3.775)$ Å changes from 21.1% (72.9%) to 29.7% (76.6%) when light intensity varies from 0 to 0.2 e/f.u.

In Fig. 3, we show data related to structural changes of the T and R phases under biaxial strain and light. Figure 3(a) demonstrates that, under dark and illumination conditions, the out-of-plane lattice constant c increases for both the T and the R phases as the in-plane lattice constant decreases. Note that a known distinction between the T and R phases is that the former has large values of c and axial ratio c/a (e.g., $c/a = 1.26$ at $a = 3.70$ Å when $n_{\mathrm{ph}} = 0$ e/f.u.), while the latter has smaller c and c/a (e.g., $c/a = 1.06$ at $a = 3.80$ Å when $n_{\mathrm{ph}} = 0$ e/f.u.), with such c/a ratios being in good agreement with experimental results for the T and R phases with the in-plane lattice constant of $a = 3.70$ and 3.80 Å, respectively [23]. Moreover, for each chosen in-plane lattice constant, the out-of-plane lattice constant for both the T and the R phases decreases when increasing the light intensity (as we will see later, such behavior reflects the fact that the out-of-plane component of the polarization is concomitantly reduced, which, in turn, makes the out-of-plane lattice constant become smaller because of the piezoelectric effect). Strikingly, this light-induced decrease of the out-of-plane lattice constant gets larger for the R phase when the in-plane lattice constant becomes smaller and gets closer to the phase transition boundary before becoming unstable (i.e., between $a = 3.72$ and 3.74 Å). For example, the decrease of the out-of-plane lattice constant at $a = 3.76$ Å is as large as 0.037 Å in the R phase for $n_{\mathrm{ph}} = 0.2$ e/f.u. The light-induced decrease of the out-of-plane lattice constant for the T phase is also getting larger but when the in-plane lattice constant increases and is within the range 3.72–3.76 Å, which is before becoming unstable. In fact, the decrease of the out-of-plane lattice constant at $a = 3.76$ Å is almost equal to that of the R phase for $n_{\mathrm{ph}} = 0.2$ e/f.u. Moreover, and as indicated in Fig. 3(b), the light-induced change of the volume for the R phase for $a = 3.76$ Å is also larger than those of other in-plane lattice constants in the R phase, which is consistent with the change of the out-of-plane lattice constant of the R phase. Similar to the R phase, the change of volume for in-plane lattice constants varying between 3.72 and 3.76 Å is larger than the others in the T phase. To quantitatively evaluate the strength of the photostriction for both the T and the R phases, we calculated the change of the out-of-plane lattice constants as a function of n_{ph} for different selected in-plane lattice constants, as shown in Figs. 3(c) and 3(d). Practically, the change of the out-of-plane lattice constant under various light intensity and for certain in-plane lattice constants is calculated via $\Delta c_{n_{\mathrm{ph}}} = \frac{c_{n_{\mathrm{ph}}} - c_{n_{\mathrm{ph}}=0}}{c_{n_{\mathrm{ph}}=0}} \times 100\%$, where $c_{n_{\mathrm{ph}}}$ and $c_{n_{\mathrm{ph}}=0}$ indicate the out-of-plane lattice constant of BFO under light

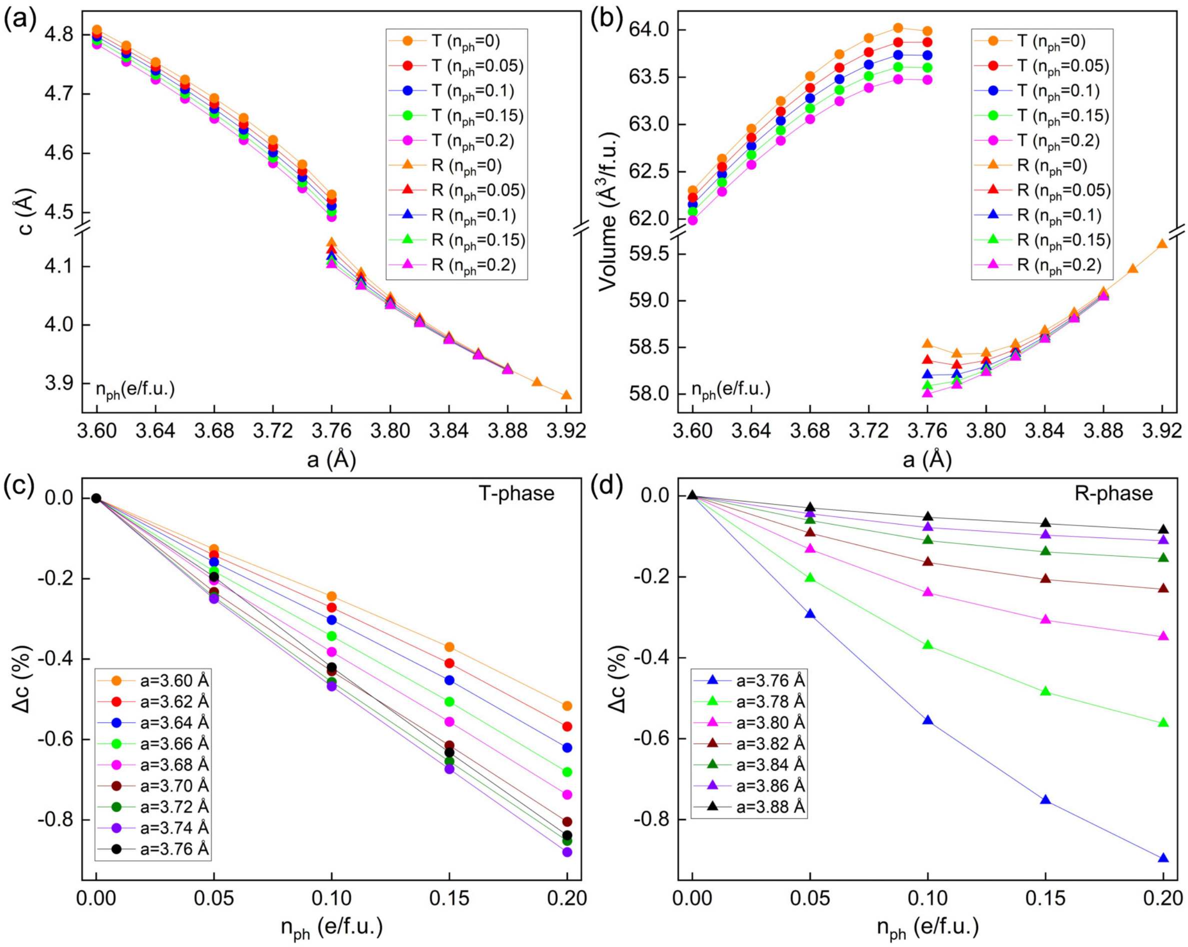

FIG. 3. Dependence of structural properties of the T and R phases of BFO films on biaxial strain and light intensity. (a) Out-of-plane lattice constant of the R and T phases as a function of the in-plane lattice constant under varying concentrations of photoexcited carrier pairs n_{ph} (e/f.u.). (b) Volume of the R and T phases as a function of the in-plane lattice constant under varying concentrations of photoexcited carrier pairs n_{ph} (e/f.u.). (c) and (d) Change in the out-of-plane lattice constant of the T and R phases, respectively, as a function of the concentration of photoexcited carrier pairs n_{ph} (e/f.u.) for different in-plane lattice constants.

and in dark, respectively. Near the phase transition boundary, the strength of the photostriction for the R and T phases can be as large as $\sim -0.9\%$ when $n_{\text{ph}} = 0.20$ e/f.u. To the best of our knowledge, such value of photostriction is one of the largest ever predicted or measured in any perovskite system. For example, it is comparable to that reported in SrCoO_3 ($\sim$1.1%) [57], SrRuO_3 ($\sim$1.12%) [15], and SrIrO_3 ($\sim$1%) [16]. We note that the light intensities that may realize the n_{ph} values we adopted in the current simulation are estimated using the model we recently proposed in Ref. [58]. The results are shown in Fig. 4. The thickness value of the BiFeO_3 film used in the model is assumed to be $d = 100$ nm, which is reported for a mixed $R + T$ phase film of BiFeO_3 [26]. The value of the absorption coefficient of BiFeO_3 is adopted as $\alpha = 2 \times 10^5\ \text{cm}^{-1}$, which is around the average value of those reported for the T and R phases of BiFeO_3 [59]. The reflection coefficient $R = 0.33$ is adopted [60]. One can see that the largest $n_{\text{ph}} = 0.2$ e/f.u. we adopted in our simulation can be realized using 400-nm-wavelength laser pulses of about 30 mJ/cm^2 for both the T and the R phases near the phase transition boundary, and thus generate a large

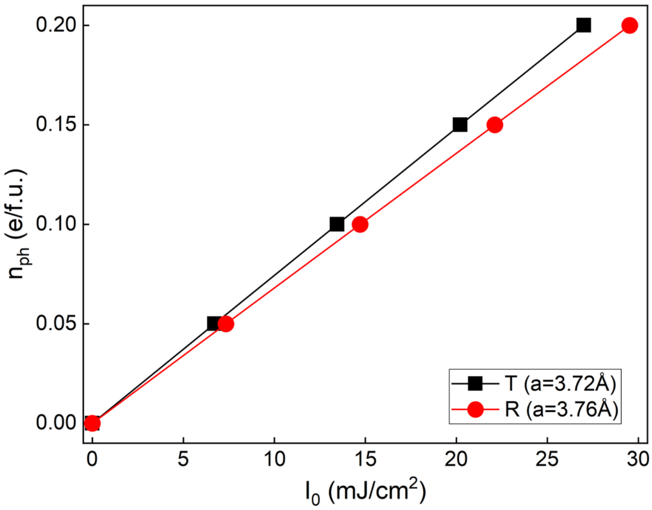

FIG. 4. Estimated photoinduced carrier concentration induced by a $\hbar\omega = 3.1$ eV (400 nm) laser pulse for the T and R phases of BiFeO_3 near the phase transition boundary that shows large photostriction. I_0 denotes the intensity of light impinging on BiFeO_3.

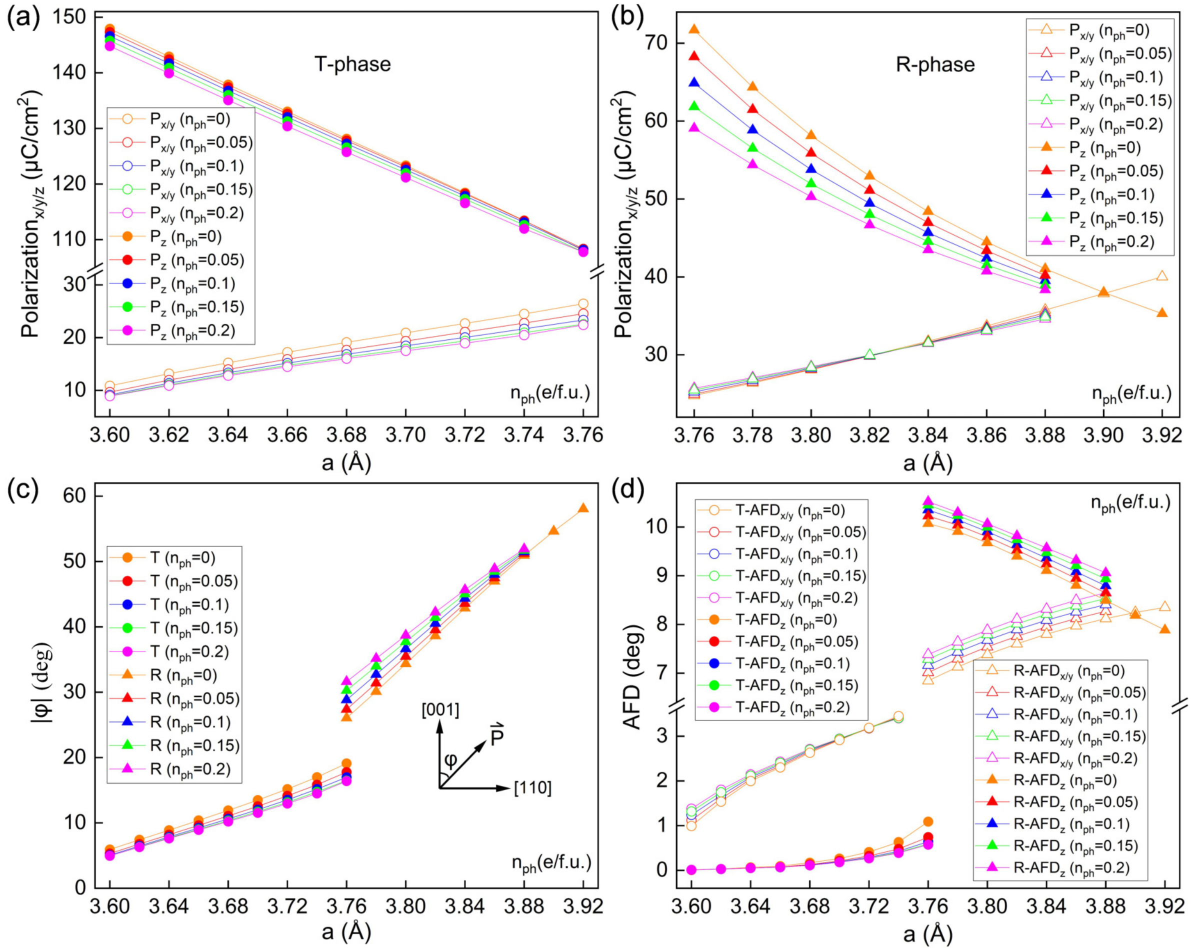

FIG. 5. (a) and (b) Electric polarization of the T and R phases, respectively, as a function of the in-plane lattice constant, for different concentrations of photoexcited carrier pairs n_{ph} (e/f.u.). (c) The angle with respect to the [001] direction made by the polarization of the R and T phases, as a function of the in-plane lattice constant for different concentrations of photoexcited carrier pairs n_{ph} (e/f.u.). (d) Antiphase tilting angles about the x and z axes in the R and T phases as a function of the in-plane lattice constant, for various concentrations of photoexcited carrier pairs n_{ph} (e/f.u.). In this latter panel, the first letter in the legends characterizes the phase (i.e., R vs T) while the last subscript represents the axis about which the antiphase tilting occurs (i.e., x/y vs z). Note that x/y indicates that we refer to either the x or the y axis, with these two axes having the same values for the component of the polarization and the tilting angle.

photostriction. In addition, the value of $\frac{\Delta c_{n_{\mathrm{ph}}}}{n_{\mathrm{ph}}}$ for the T phase at $a = 3.72$ Å and the R phase at $a = 3.76$ Å are estimated to be $-4.91\,(e/\mathrm{f.u.})^{-1}$ and $-5.86\,(e/\mathrm{f.u.})^{-1}$, respectively, at a low photoexcited carrier concentration ($n_{\mathrm{ph}} = 0.05\ e/\mathrm{f.u.}$). Compared to the calculations of unstrained bulk oxides in Table II of Ref. [58], such as $\mathrm{BiFeO_3}$, $\mathrm{BaTiO_3}$, and $\mathrm{PbTiO_3}$, the above estimated values indicate that strained $\mathrm{BiFeO_3}$ thin films exhibit superior photostriction rates near the R-T phase transition.

In order to shed more light on the combined effect of biaxial strain and light on the properties of BFO films, Fig. 5 reports the change of x and z components of the polarization, as well as the change of the antiphase tilting of the $\mathrm{FeO_6}$ octahedra [also known as antiferrodistortion (AFD) motions] about the x and z axes. Note that the x, y, and z axes are chosen along the [100], [010], and [001] pseudocubic directions, respectively, and that the y components of these two quantities are not shown here because they coincide with their x component, as a result of biaxial strain in the (x, y) plane. Technically, the polarization is calculated via the product of the Born effective charges with atomic displacements. The Born effective charges of the R and T phase structures at each in-plane lattice constant in dark conditions are adopted. We note that the Born effective charges in the R and T phase structures for different in-plane lattice constants are very similar. One can see that whether the light is applied or not on the T and R phases, decreasing the in-plane lattice constant results in reducing the in-plane components of polarization while the out-of-plane polarization's component is strengthened. Note that the T phase has mostly a rather large z component of the polarization at $a = 3.60$ Å, while the R phase has basically equal and smaller x, y, and z components at $a = 3.90$ Å, hence explaining the notation T (for tetragonal-like and for which the polarization is mostly along a pseudocubic [001] direction) and R (for rhombohedral-like and for which the polarization is near a [111] direction). For each in-plane lattice constant, increasing the concentration of the excited electrons suppresses any Cartesian component of the polarization in the T phase, and the z component of the polarization in the R phase. Such phenomenon is due to the screening effect of the excited electrons on the polarization and has been previously reported for bulk systems [35,61]. In addition, and similar to the change of the out-of-plane lattice constant depicted in Fig. 3(d), one can realize that the change of the out-of-plane polarization for the R phase under light is getting larger and larger when the in-plane lattice constant gets closer to the phase transition boundary. For the T phase, the change of the out-of-plane polarization under light is not as dramatic as that in the R phase, especially near the phase transition boundary. However, due to different dielectric susceptibilities and piezoelectric strengths, the T and R phases could present large photostriction with similar amplitudes near the phase transition. The change of the polarization direction with respect to the [001] axis under biaxial strain and light is also calculated and shown in Fig. 5(c) to further characterize changes in structural properties. Under no light, increasing the in-plane lattice constant results in the total polarization of both T and R phases deviating more and more from the [001] axis. Interestingly, applying light drives the polarization towards the [001] direction for the T phase and towards the [111] direction for the R phase, for any studied in-plane lattice constant, as a result of the fact that light more strongly reduces the x and y components of the polarization than its z component in the T phase while mostly suppressing the out-of-plane component of the polarization in the R phase. In other words, applying light makes the polarization rotate in both phases of BFO films.

Furthermore, we also calculated the antiphase tilting angles of the FeO_6 octahedra in the T and R phases of $BiFeO_3$, since it is known that such angles are typically coupled with the polarization in many perovskites, including BFO [62,63]. The results are as shown in Fig. 5(d). One can notice that, with decreasing the in-plane lattice constant from $a = 3.90$ to 3.76 Å, the in-plane AFD of the R phase decreases by a magnitude of $\sim 1.5^\circ$, while its out-of-plane AFD increases ($\sim 1.5^\circ$) for each n_{ph}. In addition, and unlike the R phase, the in-plane and out-of-plane AFD of the T phase all increases with increasing the in-plane lattice constant, but with the enhancement of the magnitude of the out-of-plane AFD being much smaller than that of the in-plane AFD. One can also see that the light-induced change of the in-plane and out-of-plane AFD of the R phase is typically larger than that of the T phase. For example, with increasing the light intensity from $n_{\mathrm{ph}} = 0$ to 0.2 e/f.u. for each calculated in-plane lattice constant from $a = 3.90$ to 3.76 Å of the R phase, the decreased (increased) magnitude of the in-plane (out-of-plane) AFD is about 0.5°. Such change in tilting angle is correlated with the aforementioned large change in the z component of the polarization, which is also accompanied by consequent changes in the out-of-plane lattice constant and volume. It is therefore important to understand the underlying mechanism responsible for such a strong photostriction effect.

For that, one has to recall that photostriction in ferroelectric materials is known to originate from the combination of three possible phenomena: converse piezoelectric effect [36,64,65], electronic pressure [66], and thermal dilation of the lattice due to heating induced by photoexcitation [67,68]. Since our DFT calculations are conducted at 0 K, we do not, implicitly, include thermal dilatation in the present investigation. We estimated the electronic pressure contribution to the total observed photostriction in the strained phase of BFO. To do that, we start with the fully relaxed structure in the dark ($n_{ph} = 0$), subsequently apply light, and fix the ionic positions, allowing only the cell to relax. By doing so, we implicitly freeze the ionic contribution to the polarization of the system, thus accounting only for the induced electronic dipole and the effect of the electronic pressure. The results are shown in Fig. 6. It is clear that the estimated contribution from the electronic pressure (black curve) is negligible for both the R and the T phases. We note that our tests (not shown here) demonstrate that the antiferromagnetic state of BFO has a lower energy than its ferromagnetic state even when the light intensity is increased to 0.2 e/f.u. Moreover, previous studies have demonstrated that the converse piezoelectric effect can be the main driving force behind photostriction in ferroelectric perovskites [35,36,61,64,65]. As such, we decided to focus on this specific effect here.

We thus first determine the light-induced change in the electrical polarization using the Born effective charges approximation, using the following equation:

$$\delta P_i = \frac{e}{\Omega} \sum_{\alpha,j} Z_{ij}^{\alpha*} \delta_j^{\alpha}, \tag{2}$$

where α runs over the ions; $i,\ j = x,\ y,\ z$ direction; δ_j^{α} is the displacement of the ion α in the j direction with respect to a reference phase and $Z_{ij}^{\alpha*}$ is the Born effective charge tensor for ion α; and Ω is the volume of the cell. Here, the reference phases correspond to the T and R phases in their ground state under dark conditions, i.e., for $n_{\mathrm{ph}} = 0$ e/f.u. (the reference phase is built for each in-plane strain considered in both phases). Notice that in doing so, we are assuming that the Born effective charges are not changed by photoexcitation [35,61]. The photoinduced strain can then be related to the change in the polarization through the following converse piezoelectric relation:

$$\delta\eta = \frac{1}{\epsilon_0} d^T \chi^{-1} \delta P, \tag{3}$$

where d^T is the transpose of the piezoelectric tensor d and χ is the dielectric susceptibility tensor. We note that the change of polarization in Eq. (3) depends on the number of generated photocarriers. Consequently, the number of generated photocarriers is taken into account in Eq. (3) via such change. Here, the dielectric susceptibility and the d tensor are computed, for each considered in-plane strain of both T and R phases. Notice that, technically, the dielectric tensor χ is obtained directly for the DFPT calculations. On the other hand, we constructed the piezoelectric tensor d from the piezoelectric e_{ij} and the elastic C_{ij} tensors, which are DFPT outputs and as implemented in the ABINIT code. First, notice that Eq. (3) can be rewritten as follows:

$$\begin{pmatrix} \delta\eta_1 \\ \delta\eta_2 \\ \delta\eta_3 \\ \delta\eta_4 \\ \delta\eta_5 \\ \delta\eta_6 \end{pmatrix} = \begin{pmatrix} d_{11} & d_{21} & d_{31} \\ d_{12} & d_{22} & d_{32} \\ d_{13} & d_{23} & d_{33} \\ d_{14} & d_{24} & d_{34} \\ d_{15} & d_{25} & d_{35} \\ d_{16} & d_{26} & d_{36} \end{pmatrix} \begin{pmatrix} \delta E_1 \\ \delta E_2 \\ \delta E_3 \end{pmatrix};\ \text{with}$$

$$\delta E_i = \frac{1}{\epsilon_0} \sum_{j=1}^{3} (\chi^{-1})_{ij} \delta P_j, \tag{4}$$

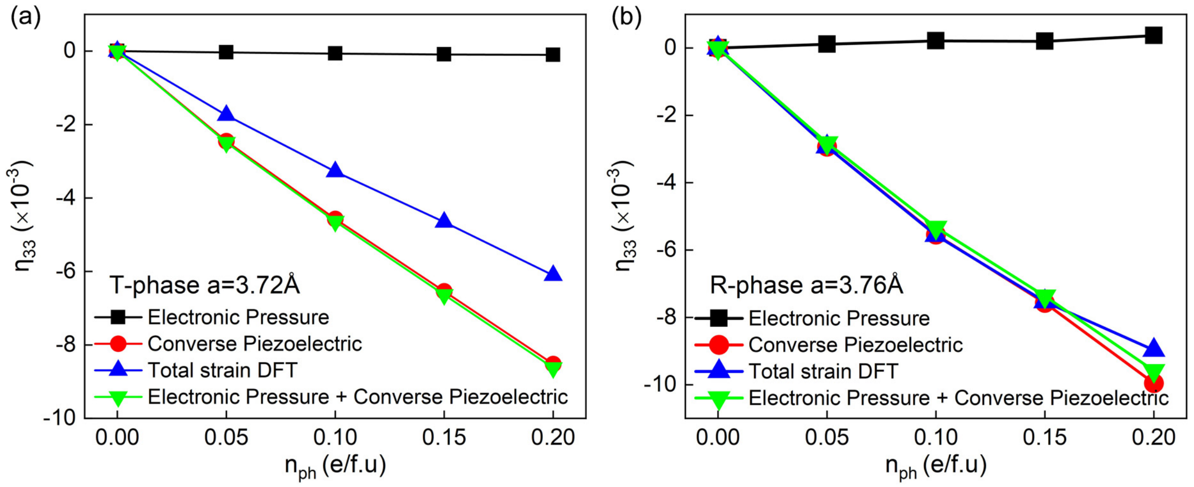

FIG. 6. Estimated electronic pressure and converse piezoelectric contribution to the total light-induced strain in the T and R phases.

where E_i is the ith component of the light-induced electric field inside the films, while i, $j = 1$, 2, and 3 indicates the x, y, and z axes, respectively.

The relaxation procedure adopted in our work imposes unclamped boundary conditions for three strains (η_3, η_4, η_5) and clamped boundary conditions for the other three (η_1, η_2, η_6). We thus restrict ourselves to (η_3, η_4, η_5) and have the following:

$$\begin{pmatrix}\delta\eta_3\\ \delta\eta_4\\ \delta\eta_5\end{pmatrix} = \begin{pmatrix}d_{13} & d_{23} & d_{33}\\ d_{14} & d_{24} & d_{34}\\ d_{15} & d_{25} & d_{35}\end{pmatrix}\begin{pmatrix}\delta E_1\\ \delta E_2\\ \delta E_3\end{pmatrix}; \text{ with}$$

$$\delta E_i = \frac{1}{\epsilon_0}\sum_{j=1}^{3}(\chi^{-1})_{ij}\delta P_j. \tag{5}$$

Now, we need to find the coefficient d_{ij} from $e_{ij} = \frac{\partial P_i}{\partial \eta_j}$ and $C_{ij} = \frac{\partial \sigma_i}{\partial \eta_j}$. Using the chain rule, the d_{ij} are obtained via the following matrix equations:

$$\frac{\partial P_i}{\partial \eta_j} = \sum_{k=3}^{5}\frac{\partial P_i}{\partial \sigma_k}\frac{\partial \sigma_k}{\partial \eta_j};\ i = 1,\ 2,\ 3;\ j = 3,\ 4,\ 5. \tag{6}$$

Equation (6) is a matrix equation:

$$\begin{pmatrix}e_{i3}\\ e_{i4}\\ e_{i5}\end{pmatrix} = \begin{pmatrix}C_{33} & C_{34} & C_{35}\\ C_{43} & C_{44} & C_{45}\\ C_{53} & C_{54} & C_{55}\end{pmatrix}\begin{pmatrix}d_{i3}\\ d_{i4}\\ d_{i5}\end{pmatrix}, \tag{7}$$

which implies that

$$\begin{pmatrix}d_{i3}\\ d_{i4}\\ d_{i5}\end{pmatrix} = \begin{pmatrix}C_{33} & C_{34} & C_{35}\\ C_{43} & C_{44} & C_{45}\\ C_{53} & C_{54} & C_{55}\end{pmatrix}^{-1}\begin{pmatrix}e_{i3}\\ e_{i4}\\ e_{i5}\end{pmatrix}. \tag{8}$$

In Fig. 7, we show the estimated strains from the converse piezoelectric model associated with Eqs (3) and (2) (in blue for the T phase and in green for the R phase) along with the direct DFT data (black for the T phase and red for the R phase) as a function of the in-plane strains and for each considered light intensity in the R and T phases. The light-induced strain is computed with respect to each phase in dark. It can be seen that the proposed model accounts for most (basically, between 80% and 95%) of the observed lattice deformation in both the R and the T phases, implying that the converse piezoelectric response dominates photostriction in BFO films. The rest of the observed deformation can likely be accounted for if one includes light-induced changes in the Born effective charges, and the light-induced changes in the dielectric and piezoelectric constants. Interestingly for the in-plane lattice near the phase transition boundary, both phases show large photoinduced strains. Notice that we are interested in the deformation along the pseudocubic c direction; thus, the values of the d_{13}, d_{23}, and d_{33} for each phase and each considered in-plane lattice constant are estimated and shown in Fig. 8. We observe that the d_{33}, for both phases, also peaks as the two phases are close to the transition boundary. This suggests, based on Eq. (3), that the dominant effect in the light-induced strain is the piezoelectric response via the d_{ij} coefficients. Therefore, it can be concluded that one should get a large photostriction close to phase transitions and/or the morphotropic phase boundary area, precisely because the piezoelectric response is large there. Note that since Eq. (3) relates the rate of change of strain to the photoinduced rate of change of the polarization δP, and not to the total polarization P, we do not expect the photostrictive effect to change sign when the polarization is reversed. In addition, the possible quadratic contributions are neglected in Eq. (3) since the model we adopted here already works well and reveals that the large photostriction originates from a piezoelectric mechanism.

We would like to point to a recent report by Ahn *et al.* [69] in which they found that the strained R and T phases of BFO expand upon optical excitation. Notice that their grown films are in open-circuit boundary condition and have polydomain structures whereas, here, we are simulating only single domain films with short-circuit boundary condition. Therefore, our work is significantly different from their report. Moreover, Ahn *et al.* only argued that the observed expansion in the strained phases shifts their relative free energies without

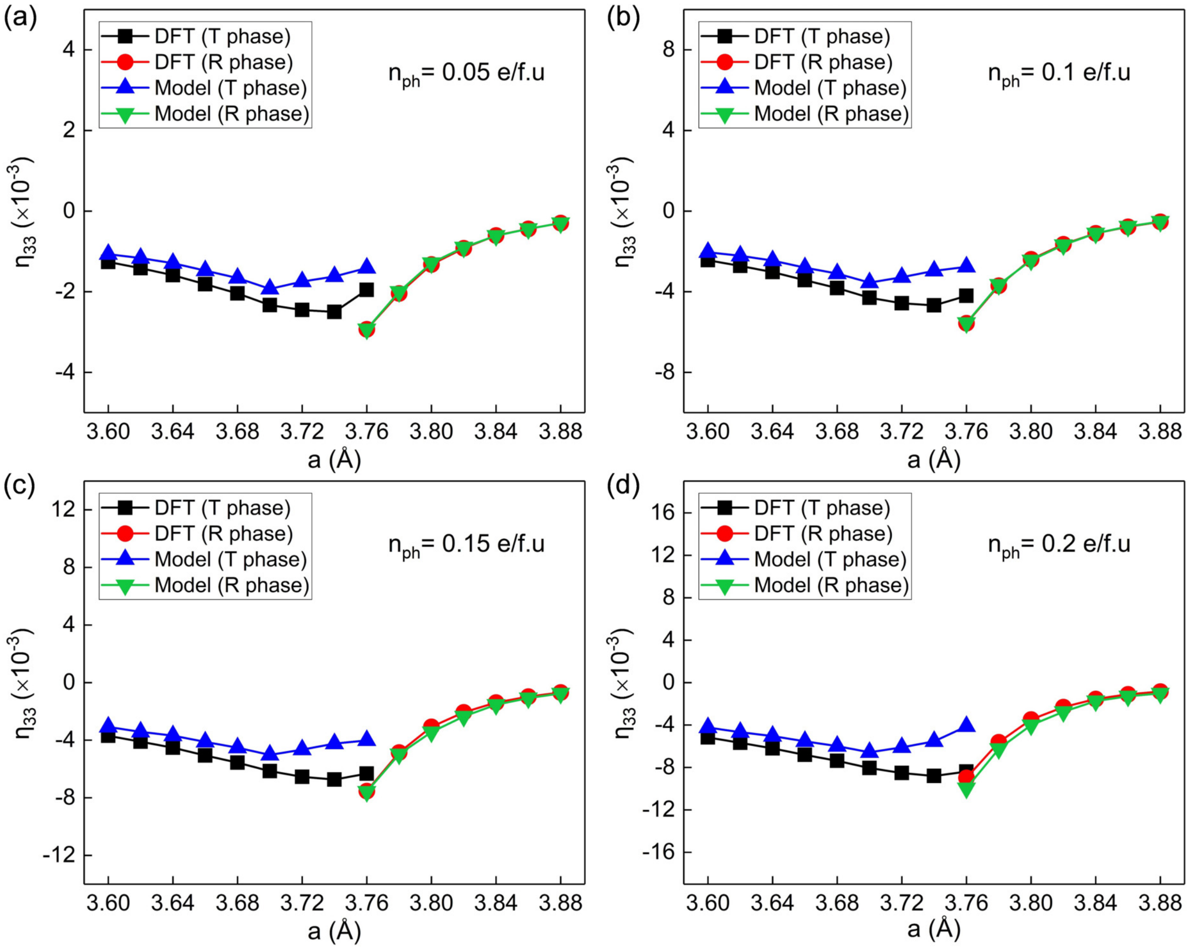

FIG. 7. Model based on the converse piezoelectric effect (denoted with the "Model" wording) vs the DFT results (indicated by the "DFT" notations) for the *R* and *T* phases of $BiFeO_3$ as a function of the in-plane lattice constant for different light intensities: (a) $n_{ph} = 0.05\ e/\mathrm{f.u.}$, (b) $n_{ph} = 0.10\ e/\mathrm{f.u.}$, (c) $n_{ph} = 0.15\ e/\mathrm{f.u.}$, and (d) $n_{ph} = 0.20\ e/\mathrm{f.u.}$

explicitly explaining the origin of the observed lattice expansion in their films. We believe that their observation is linked to the electrostatic boundary condition and possibly to the presence of domains in their films. Our work, therefore, shows that the photostrictive behavior of the strained phases of BFO is dependent on the boundary condition, which means that by controlling the electrostatic boundary conditions, one can, in principle tune the sign

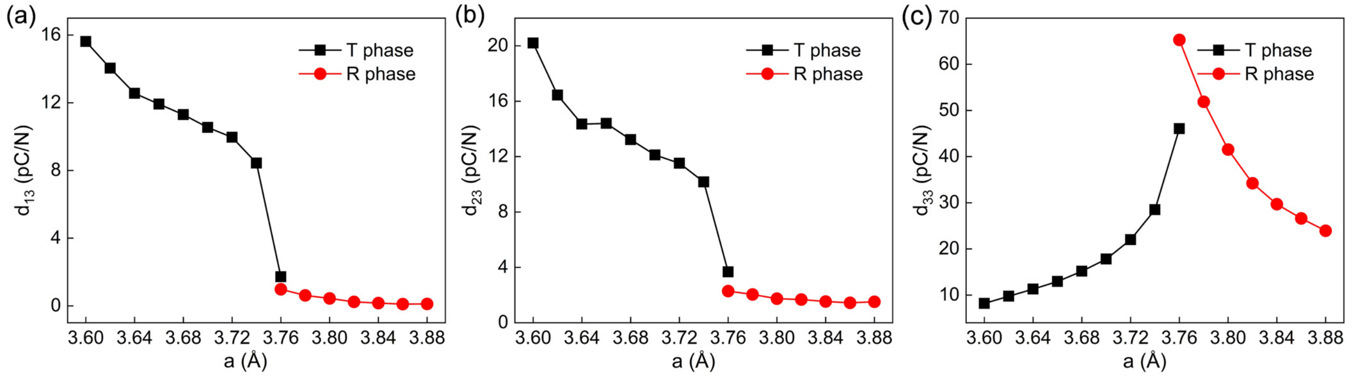

FIG. 8. Computed piezoelectric coefficients for the *R* and *T* phases with different in-plane lattice constants.

of the photostrictive response of the *R* and *T* phases of BFO.

IV. CONCLUSION

To summarize, we investigated the combined effect of biaxial strain and light on energetics, as well as structural properties of the *T* and R phases of $BiFeO_3$. The light intensity is found to have (i) little effect on the critical biaxial strain at which the (interpolated) energies of these two phases cross and (ii) a sizable effect on tuning the ratio of these two coexisting phases but only at some fixed strains, namely, corresponding to $a = 3.685$ and 3.775 Å. Importantly, a large photostriction is further found for the *R* and *T* phases near the phase transition boundary. A further developed model reveals that such large photostriction is mainly driven by the converse piezoelectric effect.

ACKNOWLEDGMENTS

Y.Y. acknowledges the support by National Natural Science Foundation of China under Grant No. 12304115 and the support by 2023 Fund for Fostering Young Scholars of the School of Mathematics and Physics, USTB under Grant No. FRF-BR-23-01B. C.D., C.P., and L.B. acknowledge the support by the Vannevar Bush Faculty Fellowship (VBFF) Grant No. N00014-20-1-2834 from the Department of Defense. L.B. also acknowledges support from ARO Grant No. W911NF-21-1-0113 and Award No. DMR-1906383 from the National Science Foundation Q-AMASE-i Program (MonArk NSF Quantum Foundry). C.P. acknowledges the support of the French Agence Nationale de la Recherche (ANR) under Grants No. ANR-21-CE24-0032 (project SUPERSPIN) and No. ANR-21-CE42-0030 (project THz-MUFINS).

---

[1] Y. Yang, W. Ren, M. Stengel, X. H. Yan, and L. Bellaiche, Revisiting properties of ferroelectric and multiferroic thin films under tensile strain from first principles, Phys. Rev. Lett. **109**, 057602 (2012).

[2] D. Edwards, N. Browne, K. M. Holsgrove, A. B. Naden, S. O. Sayedaghaee, B. Xu, S. Prosandeev, D. Wang, D. Mazumdar, M. Duchamp *et al.*, Giant resistive switching in mixed phase $BiFeO_3$ via phase population control, Nanoscale **10**, 17629 (2018).

[3] I. A. Kornev, L. Bellaiche, P. Bouvier, P. E. Janolin, B. Dkhil, and J. Kreisel, Ferroelectricity of perovskites under pressure, Phys. Rev. Lett. **95**, 196804 (2005).

[4] Z. Wu and R. E. Cohen, Pressure-induced anomalous phase transitions and colossal enhancement of piezoelectricity in $PbTiO_3$, Phys. Rev. Lett. **95**, 037601 (2005).

[5] H. J. Zhao, W. Ren, X. M. Chen, and L. Bellaiche, Effect of chemical pressure, misfit strain and hydrostatic pressure on structural and magnetic behaviors of rare-earth orthochromates, J. Phys.: Condens. Matter. **25**, 385604 (2013).

[6] L. Chen, C. Xu, H. Tian, H. Xiang, J. Íñiguez, Y. Yang, and L. Bellaiche, Electric-field control of magnetization, Jahn-Teller distortion, and orbital ordering in ferroelectric ferromagnets, Phys. Rev. Lett. **122**, 247701 (2019).

[7] P. Hemme *et al.*, Tuning the multiferroic properties of $BiFeO_3$ under uniaxial strain, Phys. Rev. Lett. **131**, 116801 (2023).

[8] S. Prosandeev, I. A. Kornev, and L. Bellaiche, Phase transitions in epitaxial (−110) $BiFeO_3$ films from first principles, Phys. Rev. Lett. **107**, 117602 (2011).

[9] H. Seo, A. Posadas, and A. A. Demkov, Strain-driven spin-state transition and superexchange interaction in $LaCoO_3$: *Ab initio* study, Phys. Rev. B **86**, 014430 (2012).

[10] C. Paillard, E. Torun, L. Wirtz, J. Íñiguez, and L. Bellaiche, Photoinduced phase transitions in ferroelectrics, Phys. Rev. Lett. **123**, 087601 (2019).

[11] M. Rini, R. Tobey, N. Dean, J. Itatani, Y. Tomioka, Y. Tokura, R. W. Schoenlein, and A. Cavalleri, Control of the electronic phase of a manganite by mode-selective vibrational excitation, Nature (London) **449**, 72 (2007).

[12] J. B. Chen, Y. Li, H. Y. Yu, Y. L. Yang, H. Jin, B. Huang, and H. J. Xiang, Light-induced magnetic phase transition in van der Waals antiferromagnets, Sci. China: Phys., Mech. Astron. **66**, 277511 (2023).

[13] E. J. Sie, C. M. Nyby, C. D. Pemmaraju, S. J. Park, X. Shen, J. Yang, M. C. Hoffmann, B. K. Ofori-Okai, R. Li, A. H. Reid *et al.*, An ultrafast symmetry switch in a Weyl semimetal, Nature (London) **565**, 61 (2019).

[14] C. Vaswani, L. L. Wang, D. H. Mudiyanselage, Q. Li, P. M. Lozano, G. D. Gu, D. Cheng, B. Song, L. Luo, R. H. J. Kim *et al.*, Light-driven Raman coherence as a nonthermal route to ultrafast topology switching in a Dirac semimetal, Phys. Rev. X **10**, 021013 (2020).

[15] T. C. Wei, H. P. Wang, H. J. Liu, D. S. Tsai, J. J. Ke, C. L. Wu, Y. P. Yin, Q. Zhan, G. R. Lin, Y. H. Chu *et al.*, Photostriction of strontium ruthenate, Nat. Commun. **8**, 15018 (2017).

[16] J. C. Yang, Y. D. Liou, W. Y. Tzeng, H. J. Liu, Y. W. Chang, P. H. Xiang, Z. Zhang, C. G. Duan, C. W. Luo, Y. C. Chen *et al.*, Ultrafast giant photostriction of epitaxial strontium iridate film with superior endurance, Nano Lett. **18**, 7742 (2018).

[17] S. Prosandeev, J. Grollier, D. Talbayev, B. Dkhil, and L. Bellaiche, Ultrafast neuromorphic dynamics using hidden phases in the prototype of relaxor ferroelectrics, Phys. Rev. Lett. **126**, 027602 (2021).

[18] J. Li, H. U. R. Strand, P. Werner, and M. Eckstein, Theory of photoinduced ultrafast switching to a spin-orbital ordered hidden phase, Nat. Commun. **9**, 4581 (2018).

[19] R. Mankowsky, A. von Hoegen, M. Forst, and A. Cavalleri, Ultrafast reversal of the ferroelectric polarization, Phys. Rev. Lett. **118**, 197601 (2017).

[20] M. M. Yang and M. Alexe, Light-induced reversible control of ferroelectric polarization in $BiFeO_3$, Adv. Mater. **30**, e1704908 (2018).

[21] P. Chen, C. Paillard, H. J. Zhao, J. Íñiguez, and L. Bellaiche, Deterministic control of ferroelectric polarization by ultrafast laser pulses, Nat. Commun. **13**, 2566 (2022).

[22] O. Dieguez, O. E. Gonzalez-Vazquez, J. C. Wojdel, and J. Íñiguez, First-principles predictions of low-energy phases of multiferroic $BiFeO_3$, Phys. Rev. B **83**, 094105 (2011).

[23] R. J. Zeches, M. D. Rossell, J. X. Zhang, A. J. Hatt, Q. He, C. H. Yang, A. Kumar, C. H. Wang, A. Melville, C. Adamo *et al.*, A strain-driven morphotropic phase boundary in $BiFeO_3$, Science **326**, 977 (2009).

[24] J. C. Wojdel and J. Íñiguez, *Ab Initio* indications for giant magnetoelectric effects driven by structural softness, Phys. Rev. Lett. **105**, 037208 (2010).

[25] J. X. Zhang, Q. He, M. Trassin, W. Luo, D. Yi, M. D. Rossell, P. Yu, L. You, C. H. Wang, C. Y. Kuo *et al.*, Microscopic origin of the giant ferroelectric polarization in tetragonal-like $BiFeO_3$, Phys. Rev. Lett. **107**, 147602 (2011).

[26] D. Sando, Y. Yang, E. Bousquet, C. Carretero, V. Garcia, S. Fusil, D. Dolfi, A. Barthelemy, P. Ghosez, L. Bellaiche *et al.*, Large elasto-optic effect and reversible electrochromism in multiferroic $BiFeO_3$, Nat. Commun. **7**, 10718 (2016).

[27] O. Paull, C. Xu, X. Cheng, Y. Zhang, B. Xu, K. P. Kelley, A. de Marco, R. K. Vasudevan, L. Bellaiche, V. Nagarajan *et al.*, Anisotropic epitaxial stabilization of a low-symmetry ferroelectric with enhanced electromechanical response, Nat. Mater. **21**, 74 (2022).

[28] Z. Huang, P. Li, Z. Fan, H. Fan, Q. Luo, C. Chen, D. Chen, M. Zeng, M. Qin, Z. Zhang *et al.*, Thickness dependence of photoconductance in strained $BiFeO_3$ thin films with planar device geometry, Phys. Status Solidi RRL **12**, 1700301 (2018).

[29] J. Zhang, X. Ke, G. Gou, J. Seidel, B. Xiang, P. Yu, W. I. Liang, A. M. Minor, Y. H. Chu, G. Van Tendeloo *et al.*, A nanoscale shape memory oxide, Nat. Commun. **4**, 2768 (2013).

[30] J. Seidel, M. Trassin, Y. Zhang, P. Maksymovych, T. Uhlig, P. Milde, D. Kohler, A. P. Baddorf, S. V. Kalinin, L. M. Eng *et al.*, Electronic properties of isosymmetric phase boundaries in highly strained Ca-doped $BiFeO_3$, Adv. Mater. **26**, 4376 (2014).

[31] Y. J. Li, J. J. Wang, J. C. Ye, X. X. Ke, G. Y. Gou, Y. Wei, F. Xue, J. Wang, C. S. Wang, R. C. Peng *et al.*, Mechanical switching of nanoscale multiferroic phase boundaries, Adv. Funct. Mater. **25**, 3405 (2015).

[32] B. Kundys, Photostrictive materials, Appl. Phys. Rev. **2**, 011301 (2015).

[33] C. Paillard, S. Prosandeev, and L. Bellaiche, *Ab initio* approach to photostriction in classical ferroelectric materials, Phys. Rev. B **96**, 045205 (2017).

[34] R. Haleoot, C. Paillard, T. P. Kaloni, M. Mehboudi, B. Xu, L. Bellaiche, and S. Barraza-Lopez, Photostrictive two-dimensional materials in the monochalcogenide family, Phys. Rev. Lett. **118**, 227401 (2017).

[35] C. Paillard, B. Xu, B. Dkhil, G. Geneste, and L. Bellaiche, Photostriction in ferroelectrics from density functional theory, Phys. Rev. Lett. **116**, 247401 (2016).

[36] M. Lejman, G. Vaudel, I. C. Infante, P. Gemeiner, V. E. Gusev, B. Dkhil, and P. Ruello, Giant ultrafast photo-induced shear strain in ferroelectric $BiFeO_3$, Nat. Commun. **5**, 4301 (2014).

[37] X. Gonze, G. M. Rignanese, M. Verstraete, J. M. Beuken, Y. Pouillon, R. Caracas, F. Jollet, M. Torrent, G. Zerah, M. Mikami *et al.*, A brief introduction to the ABINIT software package, Z. Kristallogr. **220**, 558 (2005).

[38] X. Gonze, B. Amadon, P. M. Anglade, J. M. Beuken, F. Bottin, P. Boulanger, F. Bruneval, D. Caliste, R. Caracas, M. Cote *et al.*, ABINIT: First-principles approach to material and nanosystem properties, Comput. Phys. Commun. **180**, 2582 (2009).

[39] X. Gonze, F. Jollet, F. A. Araujo, D. Adams, B. Amadon, T. Applencourt, C. Audouze, J. M. Beuken, J. Bieder, A. Bokhanchuk *et al.*, Recent developments in the ABINIT software package, Comput. Phys. Commun. **205**, 106 (2016).

[40] A. H. Romero, D. C. Allan, B. Amadon, G. Antonius, T. Applencourt, L. Baguet, J. Bieder, F. Bottin, J. Bouchet, E. Bousquet *et al.*, ABINIT: Overview and focus on selected capabilities, J. Chem. Phys. **152**, 124102 (2020).

[41] F. Jollet, M. Torrent, and N. Holzwarth, Generation of projector augmented-wave atomic data: A 71 element validated table in the XML format, Comput. Phys. Commun. **185**, 1246 (2014).

[42] V. I. Anisimov, F. Aryasetiawan, and A. I. Lichtenstein, First-principles calculations of the electronic structure and spectra of strongly correlated systems: the LDA+ U method, J. Phys.: Condens. Matter **9**, 767 (1997).

[43] A. Haykal, J. Fischer, W. Akhtar, J. Y. Chauleau, D. Sando, A. Finco, F. Godel, Y. A. Birkholzer, C. Carretero, N. Jaouen *et al.*, Antiferromagnetic textures in $BiFeO_3$ controlled by strain and electric field, Nat. Commun. **11**, 1704 (2020).

[44] I. C. Infante, S. Lisenkov, B. Dupe, M. Bibes, S. Fusil, E. Jacquet, G. Geneste, S. Petit, A. Courtial, J. Juraszek *et al.*, Bridging multiferroic phase transitions by epitaxial strain in $BiFeO_3$, Phys. Rev. Lett. **105**, 057601 (2010).

[45] W. Siemons, G. J. MacDougall, A. A. Aczel, J. L. Zarestky, M. D. Biegalski, S. Liang, E. Dagotto, S. E. Nagler, and H. M. Christen, Strain dependence of transition temperatures and structural symmetry of $BiFeO_3$ within the tetragonal-like structure, Appl. Phys. Lett. **101**, 212901 (2012).

[46] R. M. Martin, *Electronic Structure: Basic Theory and Practical Methods* (Cambridge University Press, Cambridge, 2004).

[47] S. Das Sarma and J. R. Senna, Electron-hole plasma-driven phonon renormalization in highly photoexcited GaAs, Phys. Rev. B **49**, 2443 (1994).

[48] H. Kumazoe, A. Krishnamoorthy, L. Bassman, R. K. Kalia, A. Nakano, F. Shimojo, and P. Vashishta, Photo-induced lattice contraction in layered materials, J. Phys.: Condens. Matter **30**, 32LT02 (2018).

[49] K. Liu, H. Fan, P. Ren, and C. Yang, Structural, electronic and optical properties of $BiFeO_3$ studied by first-principles, J. Alloys Compd. **509**, 1901 (2011).

[50] C. E. Dreyer, S. Coh, and M. Stengel, Nonadiabatic Born effective charges in metals and the Drude weight, Phys. Rev. Lett. **128**, 095901 (2022).

[51] B. Dupé, I. C. Infante, G. Geneste, P. E. Janolin, M. Bibes, A. Barthélémy, S. Lisenkov, L. Bellaiche, S. Ravy, and B. Dkhil, Competing phases in $BiFeO_3$ thin films under compressive epitaxial strain, Phys. Rev. B **81**, 144128 (2010).

[52] Y. D. Liou, Y. Y. Chiu, R. T. Hart, C. Y. Kuo, Y. L. Huang, Y. C. Wu, R. V. Chopdekar, H. J. Liu, A. Tanaka, C. T. Chen *et al.*, Deterministic optical control of room temperature multiferroicity in $BiFeO_3$ thin films, Nat. Mater. **18**, 580 (2019).

[53] Q. He, Y. H. Chu, J. T. Heron, S. Y. Yang, W. I. Liang, C. Y. Kuo, H. J. Lin, P. Yu, C. W. Liang, R. J. Zeches *et al.*, Electrically controllable spontaneous magnetism in nanoscale mixed phase multiferroics, Nat. Commun. **2**, 225 (2011).

[54] Y. Heo, J. Hong Lee, L. Xie, X. Pan, C.-H. Yang, and J. Seidel, Enhanced conductivity at orthorhombic–rhombohedral phase boundaries in $BiFeO_3$ thin films, NPG Asia Mater. **8**, e297 (2016).

[55] J. X. Zhang, B. Xiang, Q. He, J. Seidel, R. J. Zeches, P. Yu, S. Y. Yang, C. H. Wang, Y. H. Chu, L. W. Martin *et al.*, Large field-induced strains in a lead-free piezoelectric material, Nat. Nanotechnol. **6**, 98 (2011).

[56] Z. Chen, S. Prosandeev, Z. L. Luo, W. Ren, Y. Qi, C. W. Huang, L. You, C. Gao, I. A. Kornev, T. Wu *et al.*, Coexistence of ferroelectric triclinic phases in highly strained $BiFeO_3$ films, Phys. Rev. B **84**, 094116 (2011).

[57] B. B. Zhang *et al.*, Giant photoinduced lattice distortion in oxygen vacancy ordered $SrCoO_{2.5}$ thin films, Phys. Rev. B **100**, 144201 (2019).

[58] C. Paillard and L. Bellaiche, Light: A new handle to control the structure of cesium lead iodide, Phys. Rev. B **107**, 054107 (2023).

[59] D. Sando, C. Carrétéro, M. N. Grisolia, A. Barthélémy, V. Nagarajan, and M. Bibes, Revisiting the optical band gap in epitaxial $BiFeO_3$ thin films, Adv. Opt. Mater. **6**, 1700836 (2017).

[60] Z. Y. Zhu, S. Q. Wang, and Q. Wang, Effects of strain on optical properties of $BiFeO_3$: A first-principles study, Key Eng. Mater. **703**, 224 (2016).

[61] C. Paillard, X. Bai, I. C. Infante, M. Guennou, G. Geneste, M. Alexe, J. Kreisel, and B. Dkhil, Photovoltaics with ferroelectrics: Current status and beyond, Adv. Mater. **28**, 5153 (2016).

[62] S. Prosandeev, D. W. Wang, W. Ren, J. Íñiguez, and L. Bellaiche, Novel nanoscale twinned phases in perovskite oxides, Adv. Funct. Mater. **23**, 234 (2013).

[63] F. Xue, Y. Gu, L. Liang, Y. Wang, and L.-Q. Chen, Orientations of low-energy domain walls in perovskites with oxygen octahedral tilts, Phys. Rev. B **90**, 220101(R) (2014).

[64] B. Kundys, M. Viret, C. Meny, V. Da Costa, D. Colson, and B. Doudin, Wavelength dependence of photoinduced deformation in $BiFeO_3$, Phys. Rev. B **85**, 092301 (2012).

[65] B. Kundys, M. Viret, D. Colson, and D. O. Kundys, Light-induced size changes in $BiFeO_3$ crystals, Nat. Mater. **9**, 803 (2010).

[66] H. Wen, P. Chen, M. P. Cosgriff, D. A. Walko, J. H. Lee, C. Adamo, R. D. Schaller, J. F. Ihlefeld, E. M. Dufresne, D. G. Schlom *et al.*, Electronic origin of ultrafast photoinduced strain in $BiFeO_3$, Phys. Rev. Lett. **110**, 037601 (2013).

[67] L. Y. Chen, J. C. Yang, C. W. Luo, C. W. Laing, K. H. Wu, J. Y. Lin, T. M. Uen, J. Y. Juang, Y. H. Chu, and T. Kobayashi, Ultrafast photoinduced mechanical strain in epitaxial $BiFeO_3$ thin films, Appl. Phys. Lett. **101**, 041902 (2012).

[68] P. Ruello, T. Pezeril, S. Avanesyan, G. Vaudel, V. Gusev, I. C. Infante, and B. Dkhil, Photoexcitation of gigahertz longitudinal and shear acoustic waves in $BiFeO_3$ multiferroic single crystal, Appl. Phys. Lett. **100**, 212906 (2012).

[69] Y. Ahn *et al.*, Nanosecond optically induced phase transformation in compressively strained $BiFeO_3$ on $LaAlO_3$, Phys. Rev. Lett. **123**, 045703 (2019).